THE JOURNAL OF BIOLOGICAL CHEMISTRY VOL. 288, NO. 2, pp. 1022–1031, January 11, 2013

Structural Insights into the Inactive Subunit of the Apicoplast-localized Caseinolytic Protease Complex of *Plasmodium falciparum*[*]

Received for publication, September 4, 2012, and in revised form, November 16, 2012 Published, JBC Papers in Press, November 28, 2012, DOI 10.1074/jbc.M112.416560

Majida El Bakkouri[‡1], Sumit Rathore[§2], Charles Calmettes[‡], Amy K. Wernimont[¶], Kaiyin Liu[‡3], Dipto Sinha[§], Mohd Asad[§2], Patrick Jung[‡], Raymond Hui[¶], Asif Mohmmed[§4], and Walid A. Houry[‡5]

From the [‡]Department of Biochemistry, University of Toronto, Toronto, Ontario M5S 1A8, Canada, the [§]Malaria Group, International Centre for Genetic Engineering and Biotechnology, Aruna Asaf Ali Marg, New Delhi 110067, India, and the [¶]Structural Genomics Consortium, University of Toronto, Toronto, Ontario M5G 1L7, Canada

Background: In several organisms, caseinolytic proteases have active and inactive subunits termed ClpP and ClpR, respectively.
Results: The x-ray structure of ClpR from *Plasmodium falciparum* (*Pf*ClpR) was solved.
Conclusion: *Pf*ClpR monomer has a similar fold as ClpP but the *Pf*ClpR heptamer exhibits a more open ring than a ClpP heptamer.
Significance: This is the first structure of a ClpR subunit.

The ATP-dependent caseinolytic protease, ClpP, is highly conserved in bacteria and in the organelles of different organisms. In cyanobacteria, plant plastids, and the apicoplast of the genus *Plasmodium*, a noncatalytic paralog of ClpP, termed ClpR, has been identified. ClpRs are found to form heterocomplexes with ClpP resulting in a ClpRP tetradecameric cylinder having less than 14 catalytic triads. The exact role of ClpR in such a complex remains enigmatic. Here we describe the x-ray crystal structure of ClpR protein heptamer from *Plasmodium falciparum* (*Pf*ClpR). This is the first structure of a ClpR protein. The structure shows that the *Pf*ClpR monomer adopts a fold similar to that of ClpP, but has a unique motif, which we named the *R*-motif, forming a β turn located near the inactive catalytic triad in a three-dimensional space. The *Pf*ClpR heptamer exhibits a more open and flat ring than a ClpP heptamer. *Pf*ClpR was localized in the *P. falciparum* apicoplast as is the case of *Pf*ClpP. However, biochemical and structural data suggest that, contrary to what has been observed in other organisms, *Pf*ClpP and *Pf*ClpR do not form a stable heterocomplex in the apicoplast of *P. falciparum*.

The ATP-dependent caseinolytic proteases (Clp)[6] have essential roles in protein quality control by removing misfolded, damaged, and regulatory proteins. These proteases are highly conserved in prokaryotes, in the mitochondria of many eukaryotes, and in the chloroplast of plants (1–4). The proteases consist of a proteolytic component for protein degradation and a chaperone of the AAA^+ superfamily (5, 6) that uses ATP for substrate recognition, unfolding, and then transfer to the proteolytic component. Clp ATPase chaperones typically form hexameric complexes and contain, in addition to other domains, one (class II) or two (class I) nucleotide-binding AAA^+ domains that have characteristic Walker A and Walker B nucleotide binding and recognition motifs (5, 7–10).

The proteolytic component, termed ClpP, forms two heptameric rings resulting in a cylindrical structure (3, 11). ClpP is a serine protease containing the canonical Ser-His-Asp catalytic triad. Substrates enter the proteolytic chamber through the two axial pores located on opposite sides of the cylinder; the generated peptides of about 7 to 8 residues (12, 13) then exit the chamber through equatorial side pores that we proposed to form due to the dynamics in the structure of the ClpP complex (14–20). The AAA^+ chaperones catalyze the translocation of substrates through the ClpP axial pores and might also modulate the dynamics of the ClpP cylinder for substrate degradation and the exit of the generated peptides.

In organisms such as cyanobacteria and many plants, multiple isoforms of ClpP were found and a noncatalytic paralog of the protease, termed ClpR, was also identified (1, 3, 21, 22). ClpR has high sequence similarity to ClpP but is noncatalytic because it lacks the catalytic Ser residue, however, it was shown to be a core component of the Clp protease complex in cyanobacteria (23, 24) and plants (25). In these organisms, the Clp chaperone-protease complex typically consists of several paralogs of ClpP/ClpR and multiple ATPase chaperones. For exam-

[*] This work was supported in part by a program support grant from Department of Biotechnology, Government of India (to A. M.) and Canadian Institutes of Health Research Grant MOP-67210 (to W. A. H.).
The atomic coordinates and structure factors (codes 4GM2 and 4HNK) have been deposited in the Protein Data Bank (http://wwpdb.org/).
[1] Recipient of a fellowship from the Canadian Institutes of Health Research (CIHR) Strategic Training Program in Protein Folding and Interaction Dynamics: Principles and Diseases Grant TGF-53910.
[2] Supported by research fellowships from Indian Council of Medical Research, Government of India.
[3] Recipient of the Ontario Graduate Scholarship.
[4] Recipient of National Bioscience Award for Career Development from Department of Biotechnology, Government of India. To whom correspondence may be addressed. Tel.: 91-11-2674-1358; Fax: 91-11-2674-2316; E-mail: amohd@icgeb.res.in.
[5] To whom correspondence may be addressed. Tel.: 416-946-7141; Fax: 416-978-8548; E-mail: walid.houry@utoronto.ca.

[6] The abbreviation used is: Clp, caseinolytic proteases.

ple, the unicellular cyanobacterium *Synechococcus elongatus* has three ClpP paralogs and one ClpR. Three proteolytic core complexes were identified in *S. elongatus*: *Se*ClpP3R, *Se*ClpP1P2, and *Se*ClpP1R that interact with different AAA^+ chaperones (23). Additional studies showed that the *Se*ClpP3R cylinder consists of two identical heptameric rings of three ClpP3 and four ClpR arranged in a specific layout (24).

The Clp core complex in the plastid of *Arabidopsis thaliana* consists of five different proteolytic ClpP proteins (ClpP1, ClpP3–ClpP6) and four different ClpR proteins (ClpR1–ClpR4) (25). Recently, the subunit stoichiometry of the chloroplast *At*ClpRP tetradecameric complex was characterized by mass spectrometry and was found to have one heptameric ring consisting of ClpP3, -4, -5, -6 in a 1:2:3:1 ratio and the other heptameric ring consisting of three ClpP1s and one of each of ClpR1, -2, -3, -4 (26). Analyses of various ClpP and ClpR mutants in plants showed that the proteolytic and nonproteolytic subunits have differential contributions to the function of the complex but all of them, except for ClpR1, are essential for embryo or seedling development (21, 22).

Recent studies from our group (27, 28) demonstrated that the *Plasmodium falciparum* protozoan parasite that causes malaria in humans contains four Clp ATPases, which we termed *Pf*ClpB1, *Pf*ClpB2, *Pf*ClpC, and *Pf*ClpM, one *Pf*ClpP (gene ID PF3D7_0307400; old gene ID was PFC0310c), and one *Pf*ClpR (gene ID PF3D7_1436800; old gene ID was PF14_0348). Expression of all Clp chaperones and proteases was confirmed in blood-stage parasites. *Pf*ClpB1, *Pf*ClpC, *Pf*ClpM, and *Pf*ClpP were experimentally found to be localized in the apicoplast. *Pf*ClpB2 (also known as Hsp101) was found in the parasitophorous vacuole, whereas *Pf*ClpR was only predicted to be targeted to the apicoplast but not experimentally confirmed. Unlike the plant plastids, the apicoplast is a nonphotosynthetic organelle that does, however, accommodate several important metabolic pathways essential for parasite survival. Hence, proteins in the apicoplast are potential targets for the development of novel antimalarial drugs. Indeed, inhibiting *Pf*ClpP using β-lactones showed that the protease plays an important role in development of functional apicoplasts (28). We earlier showed that both recombinant *Pf*ClpP and *Pf*ClpR can form separate homoheptameric rings as observed by size exclusion chromatography, analytical ultracentrifugation, and electron microscopy (27, 28). However, the x-ray structure of *Pf*ClpP solved in our study showed that the protein oligomerizes as a compacted tetradecamer at high concentrations required for crystallography. No stable complexes were observed between *Pf*ClpP and *Pf*ClpR (27).

In this work, we describe the x-ray crystal structure of the *Pf*ClpR protein. This is the first structure of a ClpR protein. The structure shows that the *Pf*ClpR monomer adopts a fold similar to that of other ClpPs. However, arrangement of the *Pf*ClpR heptamer has some unique features including a more open and flat ring, as well as, the presence of a unique motif surrounding the inactive catalytic site. The biochemical and structural data indicate that both *Pf*ClpP and *Pf*ClpR are localized in the parasite apicoplast, but that they form either an unstable complex or separate complexes.

EXPERIMENTAL PROCEDURES

Parasite Culture, Plasmid Construct, and Parasite Transfection—Plasmodium falciparum strain 3D7 was cultured with human erythrocytes (4% hematocrit) in RPMI media (Invitrogen) supplemented with 10% O+ human serum using a protocol described previously (29). Parasite cultures were synchronized by repeated sorbitol treatment following the protocol of Lambros and Vanderberg (30). To generate a transfection vector construct, the full-length *PfclpR* gene (732 bp) was amplified from *P. falciparum* 3D7 genomic DNA. The amplified PCR product was then cloned in-frame to the N terminus of GFP into the vector pHH2 (31, 32). The *Pf*ClpR-GFP fragment was subcloned into the XhoI site of transfection vector $pARL1a^+$ (52) to yield construct pARL-ClpR-GFP. Synchronized *P. falciparum* 3D7 ring-stage parasites were transfected with 100 μg of purified plasmid DNA (Plasmid Maxi Kit, Qiagen) by electroporation (33), and the transfected parasites were selected over 2.5 nM WR99210 drug.

Isolation of Total DNA and RNA, cDNA Synthesis, and Quantitative Real-time PCR—The genomic DNA was isolated from an *in vitro* culture of *P. falciparum* following a standard protocol (34). Total RNAs were isolated from synchronized *P. falciparum* 3D7 parasite cultures using a mini RNA isolation kit (Qiagen). An aliquot of 50 ng of total RNA was used to synthesize cDNA using cDNA synthesis kit (Invitrogen) following the manufacturer's protocol. Gene-specific primers were designed using Beacon Designer 4.0 software, for *PfclpR*, *PfclpP*, *eba175*, and *falcipain-2* (35), and 18 S rRNA control primers were used following Blair *et al.* (36). Quantitative real-time PCR was carried out in triplicate using the iCycler version 3.0 (Bio-Rad). Each reaction contained equal amounts of cDNA, 100 ng, of both the gene-specific primers, and 1× SYBR Green PCR mix (Bio-Rad). Threshold cycle (C_t) values were calculated using iCycler software. Standard curves for each gene were obtained by using different dilutions of wild-type genomic DNA (100 to 1 ng) as template, and these standard curves were used to determine genome equivalents of C_t values for the respective gene and 18 S rRNA in each RNA sample (36). Genome equivalents of each gene were normalized using that of 18 S rRNA for all the RNA samples.

Fractionation of Parasite Lysate—Parasites were isolated from tightly synchronized *P. falciparum* 3D7 cultures at different developmental stages by lyses of infected erythrocyte with 0.15% saponin. Cell-free parasite lysate was prepared from the parasite pellet and fractionated as described earlier (28). Briefly, the parasite pellet was suspended in 1× PBS, lysed by three freeze-thaw cycles, and the lysate was clarified by centrifugation at 20,000 × *g* for 30 min at 4 °C. The cell-free extract (~5 mg protein) was fractionated on a Superose 6 HR 10/30 column (GE Healthcare) equilibrated with the lysis buffer. Eluted fractions were analyzed by Western blot using the respective antibodies. Antibodies used include: rabbit anti-*Pf*ClpP (1:1,000), rabbit anti-*Pf*ClpR (1:1,000), mice anti-GFP (1:1,000); rabbit anti-histidine-rich protein II (HRPII) (1:2,000), secondary antibody (anti-rabbit or anti-mouse, 1:2,000) conjugated to horseradish peroxidase. Bands were visualized using the ECL detection kit (GE Healthcare).

Fluorescence Microscopy and Indirect Immunofluorescence Assay—P. falciparum culture transfected with pARL-ClpR plasmid was synchronized by two sorbitol treatments. Parasites at different developmental stages were collected from the culture for fluorescence microscopy and stained with DAPI at a final concentration of 2 μg ml^{-1} and MitoTracker Red CMXRos (Invitrogen) at a final concentration of 20 nM in 1× PBS for 15 min at 37 °C. The parasites were viewed using a Nikon TE 2000-U fluorescence microscope.

Cryo-immunoelectron Microscopy—Immunoelectron microscopy was carried out on transgenic *P. falciparum* parasites expressing *Pf*ClpR-GFP at trophozoite stages as described earlier (28, 37). Parasites were fixed in 4% paraformaldehyde, 0.04% glutaraldehyde in 1× PBS at 4 °C for 1 h and, subsequently, embedded in gelatin and infiltrated with a cryo-preservative and plasticizer (2.3 M sucrose, 20% polyvinyl pyrrolidone). After freezing in liquid nitrogen, samples were sectioned with a Leica Ultracut UCT cryo-ultramicrotome (Leica Microsystems, Bannockburn, IL) at −260 °C. Ultra-thin sections were blocked with 5% fetal bovine serum and 5% normal goat serum in 1× PBS for 30 min and, subsequently, stained with rabbit anti-GFP antibody (Abcam, 1:500 dilution in blocking buffer), washed thoroughly, and then incubated with 18-nm colloidal gold-conjugated anti-rabbit IgG for 1 h. Sections were stained with 0.3% uranyl acetate, 1.7% methyl cellulose and visualized under a JEOL 1200EX transmission electron microscope (JEOL USA, Peabody, MA). All labeling experiments were conducted in parallel with controls omitting the primary antibody or using preimmune sera as primary antibodies.

*Protein Expression and Purification—Pf*ClpR constructs with N-terminal His_6 tag followed by a tobacco etch virus cut site were expressed in *Escherichia coli* SG1146, which lacks the gene coding for the endogenous *E. coli* ClpP. Cells were grown in Terrific Broth media containing 100 μg/ml of ampicillin and 34 μg/ml of chloramphenicol at 37 °C. Once the A_{600} reached 0.6, protein expression was induced by the addition of 1 mM isopropyl 1-thio-β-D-galactopyranoside. Cells were incubated overnight at 18 °C and then harvested by centrifugation and re-suspended in buffer A (50 mM Tris-HCl, pH 7.5, 300 mM NaCl, 10 mM imidazole, 10% (v/v) glycerol, and 1 mM β-mercaptoethanol). Cells were sonicated or subjected to French press and the protein was purified using a column of Ni^{2+}-nitrilotriacetic acid-agarose beads (Qiagen). After loading the sample, the column was washed in three steps using buffer A with 20, 50, and 100 mM imidazole consecutively. The protein was eluted with 500 mM imidazole. The purest fractions were pooled and dialyzed in buffer B (50 mM Tris-HCl, pH 7.5, 25 mM NaCl, 10% (v/v) glycerol, and 1 mM DTT), and subjected to ion exchange chromatography using a MonoQ column. The purest fractions were pooled once more and subjected to size exclusion chromatography using a Superdex 200 HR 10/300 GL (Amersham Biosciences) column in buffer C (10 mM HEPES, pH 7.5, and 300 mM NaCl). Fractions were pooled, concentrated, and quantified using absorbance with the following extinction coefficients: 16,515 M^{-1} cm^{-1} for *Pf*ClpR(P61-E244) and 19,495 M^{-1} cm^{-1} for *Pf*ClpR(S49-E244) obtained from the ProtParam Tools on the ExPASy Server (38).

Crystallization, Data Collection, and Processing—The hanging-drop vapor-diffusion method of crystallization was used to obtain *Pf*ClpR crystals. Initially, commercial screening kits, such as Hampton Index screen and Nextal JCSG+ Suite, were used to find a starting condition for crystallization. Single crystals were obtained for two different constructs of *Pf*ClpR: *Pf*ClpR(P61-E244) and *Pf*ClpR(S49-E244). Crystals of the first construct were obtained in crystallization conditions containing 0.1 M Tris-HCl, pH 8.5, and 20% (v/v) ethanol. Crystals of the second construct were obtained in a crystallization condition containing 0.25 M calcium acetate, pH 8.6, 7.5% PEG 20K, and 7.5% PEG MME500. 1 μl of crystallization solution was added to 1 μl of ~14 mg/ml of *Pf*ClpR protein. The reservoir contained 700 μl of crystallization solution. Crystals typically grew in 2 days at room temperature. We were not able to grow crystals in cryoprotectant condition, hence, single crystals were transferred gradually to new drops with higher concentrations of glycerol or ethylene glycol. Several such crystals were tested for x-ray diffraction. The best crystals were flash-frozen in liquid nitrogen in the presence of 25% ethylene glycol for *Pf*ClpR(P61-E244) and 10% glycerol for *Pf*ClpR(S49-E244). Diffraction data at 2.8-Å resolution were collected for crystals of *Pf*ClpR(P61-E244) at the beamline 19-ID at the Advanced Photon Source, Argonne National Laboratory. Diffraction data at 2.9-Å resolution were collected for crystals of *Pf*ClpR(S49-E244) at the CHESS A1 beamline. Data were processed and scaled with HKL2000 (39). Phaser program (53) from the CCP4 crystallographic program suite was used to search for 7 copies within the asymmetric unit. The program found 3 copies and the symmetry between two subunits was used to generate the heptamer. *Pf*ClpR structure was visualized and built using COOT (40) and refinement was done with REFMAC (41) and Phenix (42). Crystallographic details and refinement statistics are summarized in Table 1. The coordinates have been deposited in the protein structure database under the accession numbers 4GM2 for *Pf*ClpR(P61-E244) and 4HNK for *Pf*ClpR(S49-E244).

RESULTS

Localization of PfClpR in Transgenic Parasites—Initially, we carried out experiments to confirm the apicoplast localization of *Pf*ClpR. According to PlasmoDB (43), the first 49 residues of *Pf*ClpR are predicted to harbor the hydrophobic N-terminal signal sequence and the apicoplast-targeting transit peptide sequence (Fig. 1*A*). A GFP-targeting approach was employed to study the localization of *Pf*ClpR in the parasite by expressing plasmid-borne full-length *Pf*ClpR protein with a C terminally fused GFP in transgenic parasites (Fig. 1*A*). Immunoblot analysis using GFP-specific antibodies confirmed the presence of the fusion protein in trophozoite-stage transgenic parasites and not in the wild type parasite lines (Fig. 1*B*). Western blot against HRPII was used as loading control (Fig. 1*B*). Fluorescent microscopic images of the transgenic parasites at early and late trophozoite stages showed that the *Pf*ClpR-GFP fusion protein was localized in an apicoplast-like cellular organelle (Fig. 1*C*, *green*). To ascertain that the GFP fusion protein is not in the parasite mitochondria, the transgenic parasites were co-stained with MitoTracker dye, the mitochondria-specific live stain. The

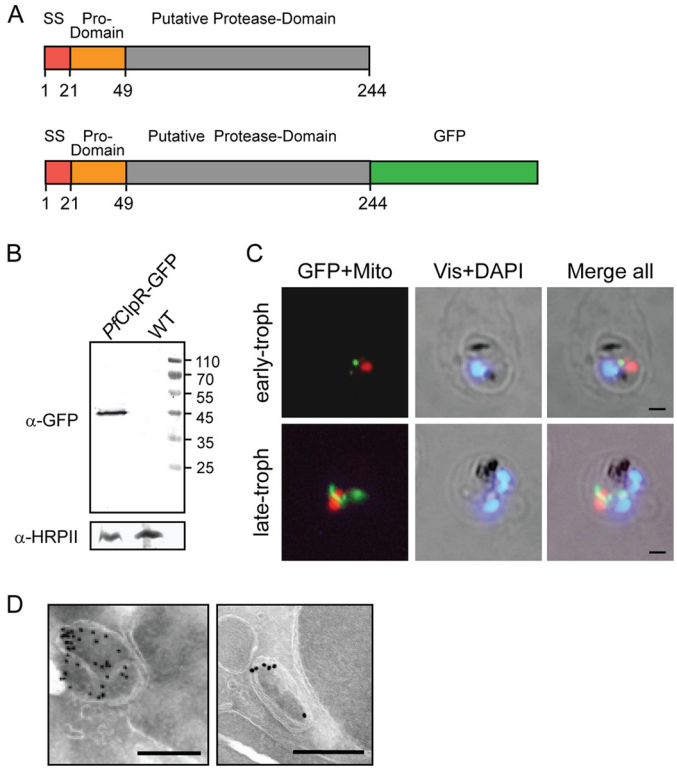

FIGURE 1. **Expression and localization of the *Pf*ClpR in transgenic parasites.** *A*, schematic domain structure of *Pf*ClpR and *Pf*ClpR-GFP showing location of signal sequence (*SS*), pro-domain, which gets cleaved off during processing, and the putative protease domain. *B*, immunoblot analysis using GFP-specific antibodies and trophozoite-stage wild type (WT) and transgenic parasites expressing *Pf*ClpR-GFP. A band of ~48 kDa, representing the GFP fusion protein, is recognized by GFP-specific antibodies in the transgenics, but not in the wild type parasite lines. A parallel blot was probed with anti-HRPII antibodies to show equal loading. *C*, fluorescent microscopic images of transgenic parasites at early and late trophozoite stages expressing *Pf*ClpR-GFP fusion protein (*green*) co-stained for live mitochondria using MitoTracker Red (*red*). The parasite nuclei were stained with DAPI (*blue*) and slides were visualized by fluorescence microscope. *Scale bar* represents 2 μm. *D*, localization of *Pf*ClpR by immunoelectron microscopy. Ultra-thin sections of transgenic *P. falciparum* parasites expressing *Pf*ClpR-GFP were labeled with anti-GFP antibody and gold-labeled secondary antibody. Labeling was observed in the apicoplast, which has the characteristic four membranes. *Scale bar* represents 250 nm.

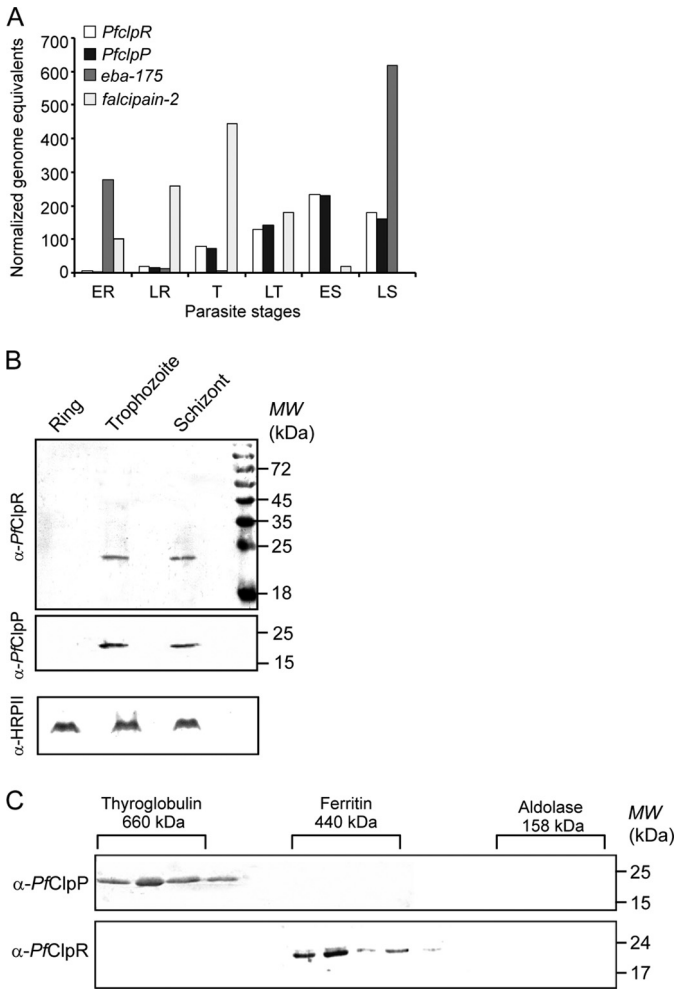

FIGURE 2. **Stage-specific expression of *Pf*ClpR in asexual blood-stage parasites.** *A*, relative transcription levels of *PfclpR* assessed by real-time RT-PCR using total RNA extracted from tightly synchronized parasite cultures at early ring (*ER*), late ring (*LR*), trophozoite (*T*), late trophozoite (*LT*), early schizont (*ES*), and late schizont (*LS*) stages (8, 16, 24, 32, 40, and 48 h after invasion, respectively). Stage-specific expression of *PfclpP*, *eba-175*, and *falcipain-2* were also analyzed. *B*, Western blot analyses of highly synchronized parasites at ring (*lane 1*), trophozoite (*lane 2*), and schizont (*lane 3*) stages with anti-*Pf*ClpR and anti-*Pf*ClpP antibodies. A parallel blot was probed with anti-HRPII antibodies to show equal loading. *C*, molecular mass of the native *Pf*ClpR and *Pf*ClpP protease complexes in the parasite. The parasite lysate was fractionated over a Superose 6 column and eluates were analyzed by Western blot using anti-*Pf*ClpR and anti-*Pf*ClpP antibodies. The elution patterns of the molecular mass standards are indicated: thyroglobulin (660 kDa), ferritin (450 kDa), and aldolase (158 kDa).

GFP fluorescence pattern (Fig. 1*C*, *green*) was observed in close association but distinct from mitochondrial staining (Fig. 1*C*, *red*). The parasite nuclei were stained with DAPI (Fig. 1*C*, *blue*). To further ascertain the localization of *Pf*ClpR-GFP fusion protein in the apicoplast, immunoelectron microscopic studies were carried out. Labeling with anti-GFP antibody followed by gold-labeled secondary antibody demonstrated the localization of the fusion protein in the lumen of the apicoplast, which was identified as a four-membrane structure in the parasite (Fig. 1*D*). From these experiments, we concluded that *Pf*ClpR is indeed localized to the apicoplast.

Analysis of the Transcription and Translation of PfClpR in the Asexual Blood-stage Parasites—The transcriptional pattern of the *PfclpR* gene in different developmental stages of the asexual blood-stage parasites was assessed by quantitative real-time PCR using total RNA samples prepared from tightly synchronized *P. falciparum* 3D7 parasite cultures at 8, 16, 30, 40, and 48 h after invasion. These results showed maximum transcription of *PfclpR* in late-trophozoite and early- and late-schizont-stage parasites (Fig. 2*A*). Maximum transcription of *PfclpP* was also observed in the same parasite stages. As control, the same set of samples were also analyzed by quantitative PCR for two other *P. falciparum* genes, erythrocyte binding antigen-175 (*eba-175*) and the cysteine protease *falcipain-2*. As expected, *eba-175* transcript levels were found to be maximum in samples from late schizont-stage parasites, whereas *falcipain-2* showed maximum transcript levels in trophozoite-stage parasites (Fig. 2*A*).

Western blot analysis of total parasite lysates detected a band of ~23 kDa in the trophozoite and schizont-stage parasites using anti-ClpR antibodies (Fig. 2*B*). This band corresponds to the calculated molecular mass of the processed *Pf*ClpR corresponding to residues ~49–244 (27) (Fig. 1*A*). No band was

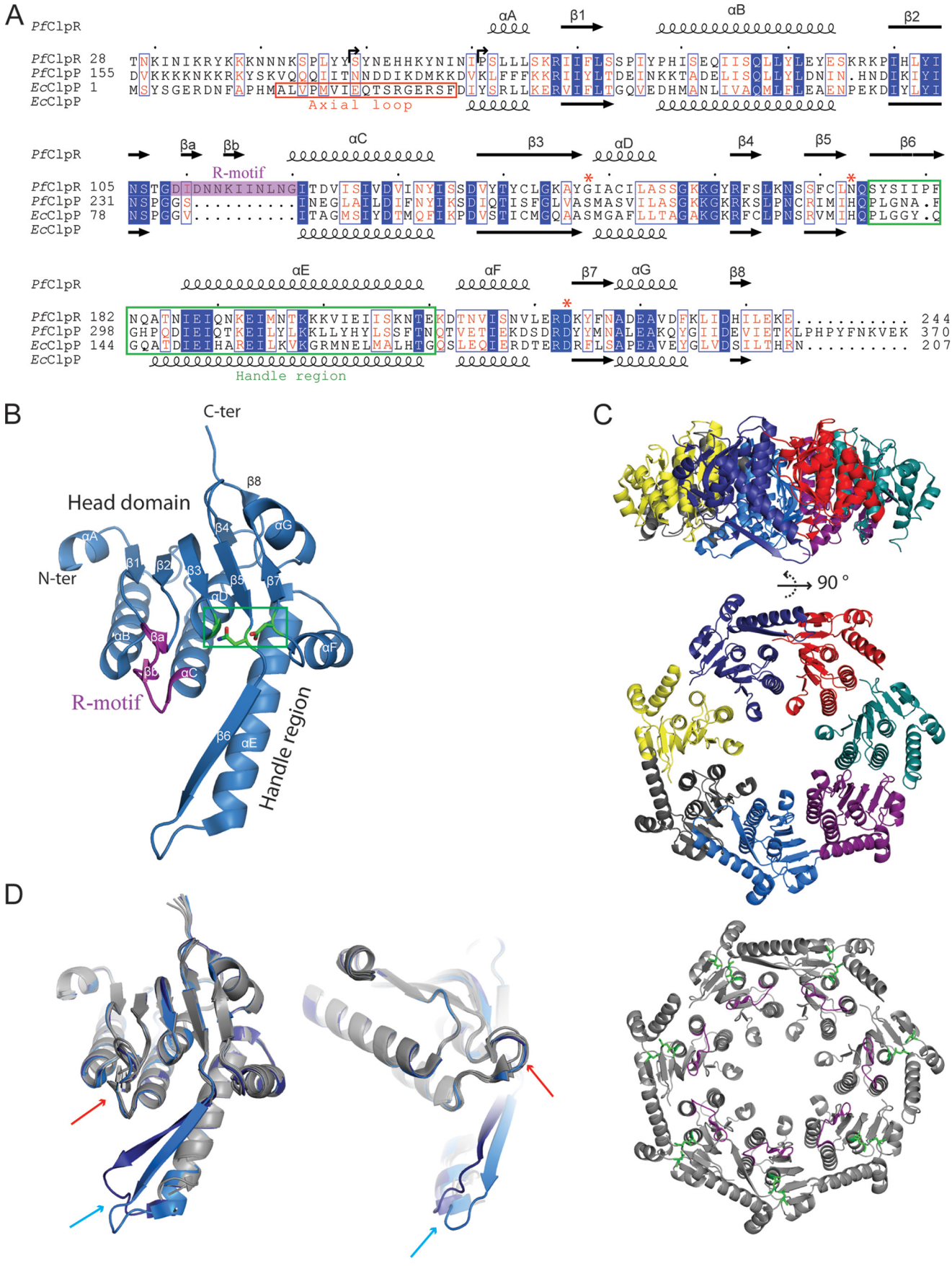

detected using preimmune sera; in addition, the anti-*Pf*ClpR antibodies did not react with the lysate of uninfected RBCs (data not shown). Western blot against HRPII was used as loading control (Fig. 2*B*). As expected anti-*PfclpP* antibodies detected a band in the trophozoite- and schizont-stage parasites. Both the transcription and translation analyses results suggest that *Pf*ClpR is expressed in blood-stage parasites at trophozoite and schizont stages, which is similar to that of *Pf*ClpP (28).

PfClpR Forms a Multisubunit Complex—To determine the size of the native protein complex of *Pf*ClpR, the parasite lysate was subjected to size exclusion chromatography using a Sepharose-6 column. The eluted samples were analyzed by Western blot using anti-*Pf*ClpR, as well as anti-*Pf*ClpP antibodies. The native *Pf*ClpR was detected in fractions of molecular mass of ~440 kDa (Fig. 2*C*). On the other hand, *Pf*ClpP eluted as a much larger complex of about 660 kDa. We had found earlier that the mature, processed *Pf*ClpP and *Pf*ClpR have similar masses of about 25 kDa (27, 28). Hence, *Pf*ClpP seems to be part of a larger complex that, unexpectedly, does not include *Pf*ClpR. This suggests that *Pf*ClpP and *Pf*ClpR do not form a stable protein complex in the parasite or that they form separate complexes.

Crystallization and Structure Determination of PfClpR—Because no structure has been reported for ClpR from any organism and to better understand the function of this inactive protease, we carried out experiments to solve the x-ray structure of *Pf*ClpR. We had shown earlier that the mature *Pf*ClpR consists approximately of residues 49–244 (Fig. 3*A*). Based on the crystal structure of ClpP from different species, residues from Ser[49] to Ile[58] of *Pf*ClpR might form flexible axial loops, which would present a challenge to crystallization. Therefore, attempts were made to crystallize both *Pf*ClpR(S49-E244) as well as *Pf*ClpR(P61-E244). The constructs contained a His_6 tag and a cut site for the tobacco etch virus protease ($MGSSH_6$SSGRENLYFQG) prior to Ser[49] or Pro[61]; these residues were not removed in the crystallization trials. Single crystals were obtained and diffracted at 2.8-Å resolution for *Pf*ClpR(P61-E244) and 2.9 Å for *Pf*ClpR(S49-E244) (Table 1). The structure was solved by molecular replacement using *Pf*ClpP protomer as template. When *Pf*ClpP heptamer was used as a template, the molecular replacement program failed to find a solution because *Pf*ClpP and *Pf*ClpR heptamers have different conformations (see below).

Overall Structure of PfClpR—Using gel filtration, analytical ultracentrifugation, and electron microscopy, we previously confirmed that *Pf*ClpR exists mainly as a heptamer in solution (27). For both constructs, *Pf*ClpR was also crystallized as a 7-fold symmetric single ring of ~106 Å in diameter and a central pore of ~30 Å (Fig. 3, *B–D*). The *Pf*ClpR(S49-E244) asymmetric unit included two 7-fold heptamers (chains A to N) related by a translational symmetry (not a double ring structure). The asymmetric unit of *Pf*ClpR(P61-E244) includes a 7-fold heptamer (chains A to G) with the same crystal packing as for *Pf*ClpR(S49-E244).

Overall, *Pf*ClpR(P61-E244) and *Pf*ClpR(S49-E244) structures are similar (Fig. 4) showing that the presence of ethanol in the crystallization condition of *Pf*ClpR(P61-E244) does not drastically affect the *Pf*ClpR structure. The root mean square deviation for the protomers is 0.66 Å and for the heptamers is 1.4 Å. Below, we will mainly refer to *Pf*ClpR(P61-E244).

This first atomic structure of a ClpR is similar to other ClpP structures with a root mean square deviation for *Pf*ClpR(P61-E244) of 1.5 Å to *Pf*ClpP and 2 Å to *Escherichia coli* ClpP (*Ec*ClpP). Each *Pf*ClpR subunit has an α/β-fold made up of six

TABLE 1
Crystallographic data collection and refinement statistics

	***Pf*ClpR(P61-E244)**	***Pf*ClpR(S49-E244)**
Data collection		
Space group	C_2	C_2
Unit cell a, b, c (Å)	182.89, 102.16, 96.41	178.79, 105.85, 186.4
α, β, γ (°)	90.00, 114.53, 90.00	90.00, 118.10, 90.00
Wavelength (Å)	0.979	0.979
Resolution (Å)	50-2.8 (2.85-2.80)	50-2.90 (2.95-2.90)
Redundancy	3.8 (3.8)	3.3 (3.0)
Completeness (%)	99.8 (100)	96.7 (87.8)
NCS redundancy	7-fold	2x7-fold
R_{merge}	0.051 (0.755)	0.075 (0.764)
I/σ(I)	27.46 (1.55)	20.07 (1.75)
Refinement	REFMAC5	PHENIX
Number of reflections used for refinement	39735	121188
Number of residues		
Amino acid residues	1202	2353
Water molecules	69	70
Glycerol	-	2
R_{cryst}	0.199	0.200
R_{free}	0.229	0.244
Average B factors (Å^2)		
Protein	102.3	89.2
Solvent	80.4	67.0
Ligand (Glycerol)	-	94.7
Wilson B factors (Å^2)	83.5	71.9
Ramachandran plot (Molprobity)		
Favored regions	96.6%	97.3%
Additional Allowed	3.1 %	2.7 %
Outliers	0.3 %	0.04 %
RMSD bond lengths/angles	0.0048Å/0.915°	0.0068Å/1.126°
PDB ID	4GM2	4HNK

Values in parentheses refer to the highest resolution shell. The various crystallographic parameters are defined as follows: R_{merge}, $\Sigma|I_i - \langle I \rangle|/\Sigma I_i$, where I_i is the intensity of the i-th observation, $\langle I \rangle$ is the mean intensity of the reflection, and the summation extends over all data. R_{cryst}, $\Sigma||F_{obs}| - |F_{calc}||/\Sigma|F_{obs}|$, where F_{obs} and F_{calc} represent, respectively, the observed and calculated structure factors. R_{free} was calculated using 5% of the observed reflections excluded from refinement. Excluded data were randomly selected.

FIGURE 3. **Domain organization of *Pf*ClpR.** *A,* sequence alignment *Ec*ClpP, *Pf*ClpP, and *Pf*ClpR using ClustalW2 (49) and visualized with ESPript (50). Residues of the Ser-His-Asp catalytic triad are indicated by a *red asterisk*. The *R*-motif is highlighted in *purple*. The handle region and axial loop are *boxed in green* and *red*, respectively. The *arrows* indicate the start site of the crystallized *Pf*ClpR proteins (following the His_6-tobacco etch virus tag). *Pf*ClpR and *Ec*ClpP secondary structures are shown on the *top* and *bottom* of the sequence alignment, respectively. Residues that are identical in the three sequences are highlighted in *blue*, whereas those that are highly similar are in *red*. *B,* ribbon diagram of *Pf*ClpR(P61-E244) protomer. The head domain and handle region are indicated. The *R*-motif is colored *purple* and the residues in the inactive catalytic triad (Gly-Asn-Asp) are shown in *green and boxed*. *C,* ribbon diagram of *Pf*ClpR(P61-E244) heptamer. In the *top two panels*, each subunit is colored differently. In the *bottom panel*, the subunits are all in *gray*, whereas the *R*-motif and the Gly-Asn-Asp sequence are colored as described in *B*. *D,* shown are overlays of the seven *Pf*ClpR(P61-E244) protomers of the heptameric ring in two different orientations. *Arrows* point to the handle region (*blue arrow*) and the *R*-motif (*red arrow*).

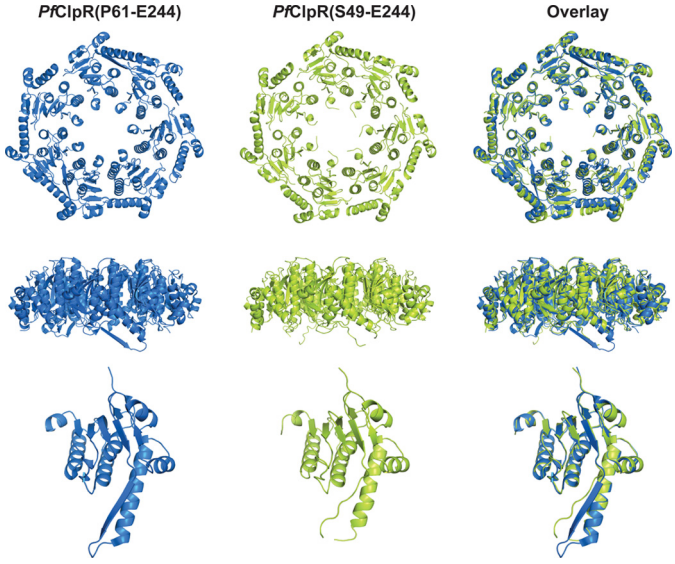

FIGURE 4. **Comparison of the *Pf*ClpR(P61-E244) and *Pf*ClpR(S49-E244) structures.** Shown is an overlay of the heptamer as well as of the protomer (subunit E) structures of *Pf*ClpR(P61-E244) (*blue*) and *Pf*ClpR(S49-E244) (*green*). From top to bottom: heptamer top view, heptamer side view, and protomer side view.

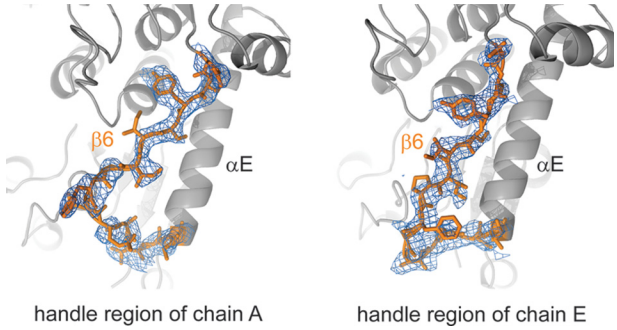

FIGURE 5. **Omit map of the handle region.** A total omit map was calculated using SFCHECK (51). Electron density contoured at 1.0 σ is shown for the handle region of chain A and chain E in *Pf*ClpR(P61-E244) structure.

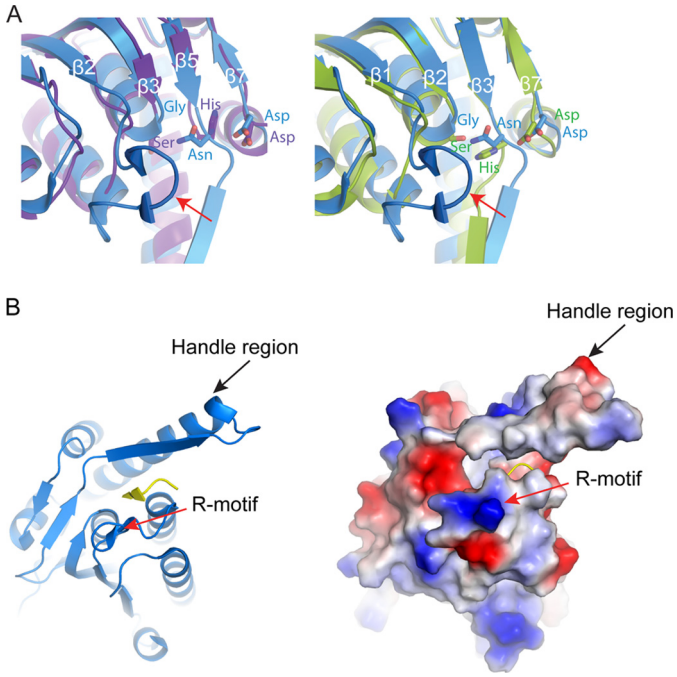

FIGURE 6. **The *Pf*ClpR inactive catalytic triad and *R*-motif.** *A*, close up view of the inactive catalytic triad, Gly-Asn-Asp of *Pf*ClpR(P61-E244) (*blue*, *both panels*) overlaid over the active catalytic triad, Ser-His-Asp, of *Pf*ClpP (*purple*, *left panel*) or *Ec*ClpP (*green*, *right panel*). The *R*-motif of *Pf*ClpR(P61-E244) is also shown indicated by a *red arrow*. *B,* superposition of the *Pf*ClpR(P61-E244) protomer structure with the structure of *Hp*ClpP protomer in complex with the heptapeptide NVLGFTQ (PDB code 2ZL2). Only the *Pf*ClpR(P61-E244) protomer (*left panel*, blue ribbon representation; *right panel*, electrostatic surface potential) and the heptapeptide (*yellow*) are shown. *Hp*ClpP is not shown.

repeats of the α/β unit (αA/β1, αB/β2, αC/β3, αD/β4/β5, αF/β7, αG/β8) forming the head domain and an additional protruding α/β unit (αE/β6) forming the handle region (Fig. 3, *A* and *B*). Residues Pro^{61}-Gln^{174} and Lys^{211}-E^{244} comprise the head domain, whereas residues Ser^{175}-Glu^{210} form the handle region. As is typically found in other ClpPs, the head domain comprises 8 β strands arranged into two layers of β sheets. On one side, the β sheets pack against a layer of α helices from the same subunit whereas, on the other side, they pack against a layer of α helices of the neighboring subunit within the heptamer (Fig. 3*C*).

We were not able to build the axial loop (Ser^{49}-Ile^{60}) of *Pf*ClpR(S49-E244) because of weak electron density. Also, the handle region is either absent or is missing some residues in all the subunits of this construct. For *Pf*ClpR(P61-E244), the final models of subunits A and E include all residues, Pro^{61}-Lys^{244}. Residues Ser^{175}-Lys^{192}, Gln^{174}-Ile^{189}, Gln^{174}-Glu^{193}, Gln^{174}-Asn^{186}, and Tyr^{176}-Ile^{187} in the handle region are missing in subunits B, C, D, F, and G, respectively. As shown in Figs. 3*D* and 5, the two handle regions that we could trace in *Pf*ClpR(P61-E244) have different orientations due to crystal packing.

The Ser-His-Asp catalytic triad is missing in *Pf*ClpR and is replaced by residues Gly^{148}-Asn^{173}-Asp^{223}, which we will call the inactive catalytic triad, which are located in a cleft between the head domain and handle region similar to the location of the catalytic triad in ClpPs (Figs. 3, *B* and *C*, and 6*A*). The head domain of *Pf*ClpR includes an insertion formed by the 10 residues Asp^{111}-Gly^{120} not present in ClpPs (Fig. 3*A*); we name Asp^{109}-Gly^{120} as the *R*-motif. The equivalent segments in *A. thaliana* and cyanobacterium *Synechococcus* have been modeled as an extension of helix C followed by a loop (24, 25). In our *Pf*ClpR structure, the *R*-motif adopts a structured β turn that is largely equivalent in all 7 subunits (Fig. 3*D*) and protrudes from the head domain without affecting the α/β-fold (Fig. 3*D*). It also includes an extension of helix C (residues NG). The *R*-motif is adjacent to the presumed active site and faces the internal chamber of the heptamer (Fig. 6*A*).

In ClpP, each subunit has a hydrophobic groove forming a continuous substrate-binding surface leading to the catalytic triad (44, 45). An examination of surface topology and surface potential of *Pf*ClpR reveals that this groove is present in the *Pf*ClpR structure and is formed by residues Ile^{121}, Ile^{149}, Ile^{152}, Leu^{172}, Asn^{173}, Ser^{175}, Val^{201}, Ile^{205}, and Leu^{220} (Fig. 6, *A* and *B*). The presence of the *R*-motif results in the formation of a deep cleft without significantly restricting accessibility to the groove from the internal chamber of the *Pf*ClpR heptamer (Fig. 6*B*). This is clearly observed if the *Pf*ClpR structure is overlaid with the structure of the *Helicobacter pylori* ClpP protomer

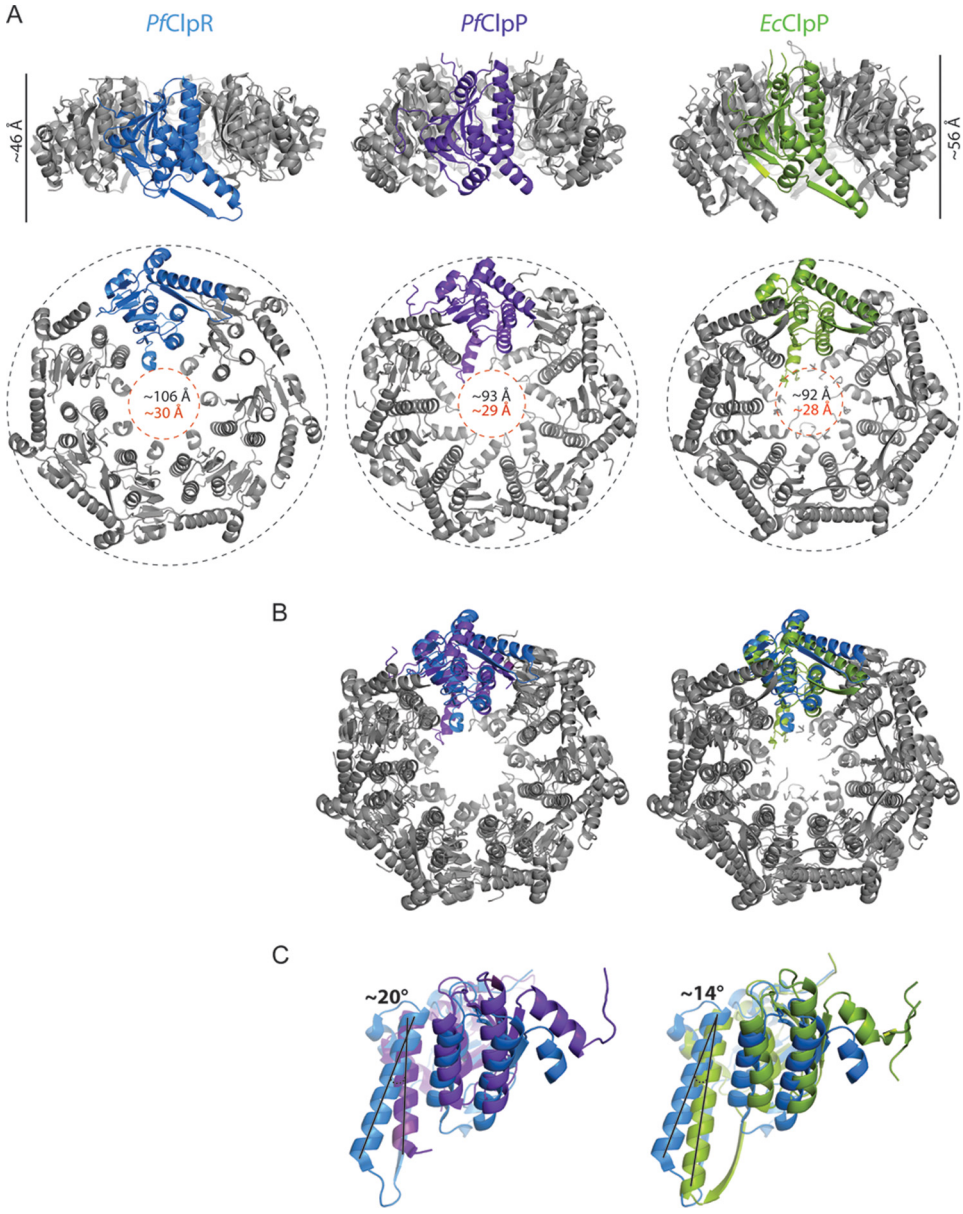

FIGURE 7. **PfClpR heptamer organization.** *A,* ribbon diagram of *Pf*ClpR(P61-E244), *Pf*ClpP, and *Ec*ClpP, respectively, viewed from the side (*top panel*) and top (*bottom panel*). The heptamers are colored *gray* except for one subunit of *Pf*ClpR(P61-E244), *Pf*ClpP and *Ec*ClpP are colored *blue*, *purple*, and *green*, respectively. The dimensions shown were measured from the two-dimensional projections of the proteins. *B*, overlay of the *Pf*ClpR(P61-E244) heptamer with *Pf*ClpP heptamer (*left*) and *Ec*ClpP heptamer (*right*). The colors are as in *A*. *C,* shown is the overlay of one protomer from the heptamer overlays shown in *B*.

that is in complex with a heptapeptide NVLGFTQ (PDB code 2ZL2). The heptapeptide is found to nicely fit into that deep cleft of *Pf*ClpR (Fig. 6*B*). The amino acid sequence of the *R*-motif is highly conserved in the genus *Plasmodium* with a consensus sequence of: D(I/L)(D/E)NNKI(I/V)NLNG. This suggests that the motif may play an essential role related to the function of this protein.

The Oligomerization of PfClpR—The *Pf*ClpR(P61-E244) heptamer is stabilized by extensive interactions among the head domains with about 30% of the total surface area making contacts within the heptamer. Compared with *Ec*ClpP and *Pf*ClpP structures, the *Pf*ClpR(P61-E244) heptamer is compressed by about 10 Å along the *z* axis and is wider by about 14 Å along the *x* axis (Fig. 7*A*). This is the result of a twist of each subunit in the *Pf*ClpR(P61-E244) heptamer by about 15° outwards leading to a more open structure of the *Pf*ClpR(P61-E244) heptamer (Fig. 7, *B* and *C*). As a consequence of the open shape of *Pf*ClpR(P61-E244), the surface area of the heptameric complex is larger than that of *Pf*ClpP or *Ec*ClpP: ~56,630 Å^2 for *Pf*ClpR(P61-E244), ~46430 Å^2 for *Pf*ClpP, and ~50,970 Å^2 for *Ec*ClpP. This observation leads us to conclude that a flat ring of *Pf*ClpR is probably not favorable for an interaction with the *Pf*ClpP ring, unless a conformational change in *Pf*ClpR is induced. This might explain our inability to observe a stable *Pf*ClpRP complex using the purified proteins (27).

DISCUSSION

In eukaryotes, the 26 S proteasome plays an essential role in controlling the levels of key regulatory proteins and in degrading abnormal polypeptides; it also plays a key role in cell cycle

progression and the regulation of numerous transcription factors (46). In prokaryotes, mitochondria, and plant chloroplasts, these tasks are carried out by the Clp chaperone-protease system (47). We had earlier identified and characterized the Clp chaperones and proteases in *P. falciparum* (27, 28, 48). In this study, we have experimentally confirmed that, like *Pf*ClpP, *Pf*ClpR is localized in the apicoplast of the parasite (Fig. 1, *C* and *D*). Furthermore, both proteins were found to be expressed in blood-stage parasites at trophozoite and schizont stages (Fig. 2, *A* and *B*, and Ref. 27 and 28) suggesting that they might function together. However, it was surprising to find that the two proteins do not co-elute when a *P. falciparum* lysate is fractionated (Fig. 2*C*).

We also determined the crystal structure of *Pf*ClpR protein, which exists as a heptamer in solution (27). Although the structure of *Pf*ClpR monomer is similar to that of *Pf*ClpP (Figs. 3*D* and 7*C*), the dimensions and shapes of *Pf*ClpP and *Pf*ClpR heptameric rings are different (Figs. 4 and 7, *A* and *B*). The structure we obtained for *Pf*ClpR showed a flattened heptameric complex compared with that of ClpP (Fig. 7*A*) that is unlikely to be able to interact stably with an equivalent heptameric *Pf*ClpP by the intercalation of the handle regions as typically observed in ClpP tetradecamers. These results correlate with the presence of separate *Pf*ClpR and *Pf*ClpP complexes in the parasite as observed in the size exclusion fractionation experiment (Fig. 2*C*). However, at this stage, we cannot exclude the possibility that a AAA^+ chaperone or some other cofactor might induce a conformational change in *Pf*ClpR or *Pf*ClpP to allow for the formation of a transient tetradecameric complex consisting of two homo-heptameric rings $PfClpR_7$-$PfClpP_7$. The presence of a substrate might also stabilize a $PfClpR_7$-$PfClpP_7$ complex. Alternatively, a functional hetero-heptameric *Pf*ClpRP complex in the apicoplast may be present at very low levels to be detected by the fractionation experiment of Fig. 2*C*; however, we have not yet been able to form such a complex *in vitro*. It should be noted that *Pf*ClpP formed a tetradecamer in the crystal but a heptamer in solution (27), indicating a concentration-dependent oligomerization.

If indeed *Pf*ClpR and *Pf*ClpP do not form a complex in the apicoplast of *Plasmodium*, then this suggests the presence of a separate inactive *Pf*ClpR complex with distinct activities from *Pf*ClpP. *Pf*ClpR might indirectly regulate the activity of *Pf*ClpP by competing for interactions with cognate AAA^+ proteins. Alternatively, the *Pf*ClpR ring might have a chaperone-like activity. This is suggested by the presence of the deep hydrophobic clefts formed by the *R*-motif and the substrate-binding surface leading to the inactive catalytic triad (Fig. 6). Exposed hydrophobic segments in unfolded or misfolded proteins can bind in these clefts. However, it should be pointed out that these possible alternative functions for *Pf*ClpR would be specific for apicomplexa and would not be consistent with the fact that hetero-oligomeric complexes have been observed in plant plastids and cyanobacteria.

It should be noted that, whereas the *R*-motif seems to be present in most of the cyanobacterial and plant ClpRs, the amino acid sequence of the motif is not conserved across species. Furthermore, some ClpRs have other insertions as well. For example, *Se*ClpR has an insertion between β1 and αB, which is not present in plant or *Plasmodium* ClpRs (24, 25, 27). The role of such insertions is not known; these insertions might be required to further optimize or modify the function of the protein in a species-specific manner.

In conclusion, our study provides the first structure of a ClpR protein. The structure helps to further our understanding of the role that ClpR plays in different organisms. However, the function of *Pf*ClpR in *Plasmodium* and the possible presence of a *Pf*ClpRP complex remains enigmatic and requires additional studies.

Acknowledgments—We are grateful to Alan Cowman (Walter and Eliza Hall Institute of Medical Research, Australia) for pARL1 vector, and Guy Schiehser and David Jacobus (Jacobus Pharmaceuticals, NJ, USA) for the drug WR99210. We thank Wandy Beatty for help with the immunoelectron microscopic studies and the Rotary Blood Bank, New Delhi, for providing the human RBCs.

REFERENCES

1. Adam, Z., Rudella, A., and van Wijk, K. J. (2006) Recent advances in the study of Clp, FtsH and other proteases located in chloroplasts. *Curr. Opin. Plant Biol.* **9,** 234–240
2. Sakamoto, W. (2006) Protein degradation machineries in plastids. *Annu. Rev. Plant Biol.* **57,** 599–621
3. Yu, A. Y., and Houry, W. A. (2007) ClpP. A distinctive family of cylindrical energy-dependent serine proteases. *FEBS Lett.* **581,** 3749–3757
4. Kress, W., Maglica, Z., and Weber-Ban, E. (2009) Clp chaperone-proteases. Structure and function. *Res. Microbiol.* **160,** 618–628
5. Neuwald, A. F., Aravind, L., Spouge, J. L., and Koonin, E. V. (1999) AAA^+. A class of chaperone-like ATPases associated with the assembly, operation, and disassembly of protein complexes. *Genome Res.* **9,** 27–43
6. Snider, J., Thibault, G., and Houry, W. A. (2008) The AAA^+ superfamily of functionally diverse proteins. *Genome Biol.* **9,** 216
7. Dougan, D. A., Mogk, A., Zeth, K., Turgay, K., and Bukau, B. (2002) AAA^+ proteins and substrate recognition, it all depends on their partner in crime. *FEBS Lett.* **529,** 6–10
8. Iyer, L. M., Leipe, D. D., Koonin, E. V., and Aravind, L. (2004) Evolutionary history and higher order classification of AAA^+ ATPases. *J. Struct. Biol.* **146,** 11–31
9. Ammelburg, M., Frickey, T., and Lupas, A. N. (2006) Classification of AAA^+ proteins. *J. Struct. Biol.* **156,** 2–11
10. Snider, J., and Houry, W. A. (2008) AAA^+ proteins. Diversity in function, similarity in structure. *Biochem. Soc. Trans.* **36,** 72–77
11. Baker, T. A., and Sauer, R. T. (2012) ClpXP, an ATP-powered unfolding and protein-degradation machine. *Biochim. Biophys. Acta* **1823,** 15–28
12. Choi, K. H., and Licht, S. (2005) Control of peptide product sizes by the energy-dependent protease ClpAP. *Biochemistry* **44,** 13921–13931
13. Jennings, L. D., Lun, D. S., Médard, M., and Licht, S. (2008) ClpP hydrolyzes a protein substrate processively in the absence of the ClpA ATPase. Mechanistic studies of ATP-independent proteolysis. *Biochemistry* **47,** 11536–11546
14. Gribun, A., Kimber, M. S., Ching, R., Sprangers, R., Fiebig, K. M., and Houry, W. A. (2005) The ClpP double ring tetradecameric protease exhibits plastic ring-ring interactions, and the N termini of its subunits form flexible loops that are essential for ClpXP and ClpAP complex formation. *J. Biol. Chem.* **280,** 16185–16196
15. Sprangers, R., Gribun, A., Hwang, P. M., Houry, W. A., and Kay, L. E. (2005) Quantitative NMR spectroscopy of supramolecular complexes. Dynamic side pores in ClpP are important for product release. *Proc. Natl. Acad. Sci. U.S.A.* **102,** 16678–16683
16. Kimber, M. S., Yu, A. Y., Borg, M., Leung, E., Chan, H. S., and Houry, W. A. (2010) Structural and theoretical studies indicate that the cylindrical protease ClpP samples extended and compact conformations. *Structure* **18,** 798–808

17. Geiger, S. R., Böttcher, T., Sieber, S. A., and Cramer, P. (2011) A conformational switch underlies ClpP protease function. *Angew. Chem. Int. Ed. Engl.* **50,** 5749–5752
18. Lee, B. G., Kim, M. K., and Song, H. K. (2011) Structural insights into the conformational diversity of ClpP from *Bacillus subtilis*. *Mol. Cells* **32,** 589–595
19. Zhang, J., Ye, F., Lan, L., Jiang, H., Luo, C., and Yang, C. G. (2011) Structural switching of *Staphylococcus aureus* Clp protease. A key to understanding protease dynamics. *J. Biol. Chem.* **286,** 37590–37601
20. Gersch, M., List, A., Groll, M., and Sieber, S. A. (2012) Insights into structural network responsible for oligomerization and activity of bacterial virulence regulator caseinolytic protease P (ClpP) protein. *J. Biol. Chem.* **287,** 9484–9494
21. Kato, Y., and Sakamoto, W. (2010) in *International Review of Cell and Molecular Biology* (Kwang, W. J., ed) pp. 185–218, Academic Press, New York
22. Olinares, P. D., Kim, J., and van Wijk, K. J. (2011) The Clp protease system. A central component of the chloroplast protease network. *Biochim. Biophys. Acta* **1807,** 999–1011
23. Stanne, T. M., Pojidaeva, E., Andersson, F. I., and Clarke, A. K. (2007) Distinctive types of ATP-dependent Clp proteases in cyanobacteria. *J. Biol. Chem.* **282,** 14394–14402
24. Andersson, F. I., Tryggvesson, A., Sharon, M., Diemand, A. V., Classen, M., Best, C., Schmidt, R., Schelin, J., Stanne, T. M., Bukau, B., Robinson, C. V., Witt, S., Mogk, A., and Clarke, A. K. (2009) Structure and function of a novel type of ATP-dependent Clp protease. *J. Biol. Chem.* **284,** 13519–13532
25. Peltier, J. B., Ripoll, D. R., Friso, G., Rudella, A., Cai, Y., Ytterberg, J., Giacomelli, L., Pillardy, J., and van Wijk, K. J. (2004) Clp protease complexes from photosynthetic and non-photosynthetic plastids and mitochondria of plants, their predicted three-dimensional structures, and functional implications. *J. Biol. Chem.* **279,** 4768–4781
26. Olinares, P. D., Kim, J., Davis, J. I., and van Wijk, K. J. (2011) Subunit stoichiometry, evolution, and functional implications of an asymmetric plant plastid ClpP/R protease complex in *Arabidopsis*. *Plant Cell* **23,** 2348–2361
27. El Bakkouri, M., Pow, A., Mulichak, A., Cheung, K. L., Artz, J. D., Amani, M., Fell, S., de Koning-Ward, T. F., Goodman, C. D., McFadden, G. I., Ortega, J., Hui, R., and Houry, W. A. (2010) The Clp chaperones and proteases of the human malaria parasite *Plasmodium falciparum*. *J. Mol. Biol.* **404,** 456–477
28. Rathore, S., Sinha, D., Asad, M., Böttcher, T., Afrin, F., Chauhan, V. S., Gupta, D., Sieber, S. A., and Mohmmed, A. (2010) A cyanobacterial serine protease of *Plasmodium falciparum* is targeted to the apicoplast and plays an important role in its growth and development. *Mol. Microbiol.* **77,** 873–890
29. Trager, W., and Jensen, J. B. (1976) Human malaria parasites in continuous culture. *Science* **193,** 673–675
30. Lambros, C., and Vanderberg, J. P. (1979) Synchronization of *Plasmodium falciparum* erythrocytic stages in culture. *J. Parasitol.* **65,** 418–420
31. Reed, M. B., Caruana, S. R., Batchelor, A. H., Thompson, J. K., Crabb, B. S., and Cowman, A. F. (2000) Targeted disruption of an erythrocyte binding antigen in *Plasmodium falciparum* is associated with a switch toward a sialic acid-independent pathway of invasion. *Proc. Natl. Acad. Sci. U.S.A.* **97,** 7509–7514
32. Waller, R. F., Reed, M. B., Cowman, A. F., and McFadden, G. I. (2000) Protein trafficking to the plastid of *Plasmodium falciparum* is via the secretory pathway. *EMBO J.* **19,** 1794–1802
33. Crabb, B. S., Rug, M., Gilberger, T. W., Thompson, J. K., Triglia, T., Maier, A. G., and Cowman, A. F. (2004) Transfection of the human malaria parasite *Plasmodium falciparum*. *Methods Mol. Biol.* **270,** 263–276
34. Ljungström, I., Perlmann, H., Schlichtherle, M., Scherf, A., and Wahlgren, M. (2004) *Methods in Malaria Research*, MR4/ATCC, Manassas, VA
35. Dasaradhi, P. V., Mohmmed, A., Kumar, A., Hossain, M. J., Bhatnagar, R. K., Chauhan, V. S., and Malhotra, P. (2005) A role of falcipain-2, principal cysteine proteases of *Plasmodium falciparum* in merozoite egression. *Biochem. Biophys. Res. Commun.* **336,** 1062–1068
36. Blair, P. L., Witney, A., Haynes, J. D., Moch, J. K., Carucci, D. J., and Adams, J. H. (2002) Transcripts of developmentally regulated *Plasmodium falciparum* genes quantified by real-time RT-PCR. *Nucleic Acids Res.* **30,** 2224–2231
37. Wickramarachchi, T., Devi, Y. S., Mohmmed, A., and Chauhan, V. S. (2008) Identification and characterization of a novel *Plasmodium falciparum* merozoite apical protein involved in erythrocyte binding and invasion. *PLoS One* **3,** e1732
38. Gasteiger, E., Hoogland, C., A., G., Duvaud, S., Wilkins, M. R., Appel, R. D., and Bairoch, A. (2005) in *The Proteomics Protocols Handbook* (Walker, J. M., ed) pp. 571–607, Humana Press, New York
39. Otwinowski, Z., and Minor, W. (1997) Processing of x-ray diffraction data collected in oscillation mode. *Methods Enzymol.* **276,** 307–326
40. Emsley, P., and Cowtan, K. (2004) Coot. Model-building tools for molecular graphics. *Acta Crystallogr. D Biol. Crystallogr.* **60,** 2126–2132
41. Murshudov, G. N., Vagin, A. A., and Dodson, E. J. (1997) Refinement of macromolecular structures by the maximum-likelihood method. *Acta Crystallogr. D Biol. Crystallogr.* **53,** 240–255
42. Adams, P. D., Afonine, P. V., Bunkóczi, G., Chen, V. B., Davis, I. W., Echols, N., Headd, J. J., Hung, L. W., Kapral, G. J., Grosse-Kunstleve, R. W., McCoy, A. J., Moriarty, N. W., Oeffner, R., Read, R. J., Richardson, D. C., Richardson, J. S., Terwilliger, T. C., and Zwart, P. H. (2010) PHENIX. A comprehensive Python-based system for macromolecular structure solution. *Acta Crystallogr. D Biol. Crystallogr.* **66,** 213–221
43. Aurrecoechea, C., Brestelli, J., Brunk, B. P., Dommer, J., Fischer, S., Gajria, B., Gao, X., Gingle, A., Grant, G., Harb, O. S., Heiges, M., Innamorato, F., Iodice, J., Kissinger, J. C., Kraemer, E., Li, W., Miller, J. A., Nayak, V., Pennington, C., Pinney, D. F., Roos, D. S., Ross, C., Stoeckert, C. J., Jr., Treatman, C., and Wang, H. (2009) PlasmoDB. A functional genomic database for malaria parasites. *Nucleic Acids Res.* **37,** D539–543
44. Wang, J., Hartling, J. A., and Flanagan, J. M. (1997) The structure of ClpP at 2.3-Å resolution suggests a model for ATP-dependent proteolysis. *Cell* **91,** 447–456
45. Kim, D. Y., and Kim, K. K. (2008) The structural basis for the activation and peptide recognition of bacterial ClpP. *J. Mol. Biol.* **379,** 760–771
46. Ciechanover, A. (2012) Intracellular protein degradation. From a vague idea thru the lysosome and the ubiquitin-proteasome system and onto human diseases and drug targeting. *Biochim. Biophys. Acta* **1824,** 3–13
47. De Mot, R., Nagy, I., Walz, J., and Baumeister, W. (1999) Proteasomes and other self-compartmentalizing proteases in prokaryotes. *Trends Microbiol.* **7,** 88–92
48. Ramasamy, G., Gupta, D., Mohmmed, A., and Chauhan, V. S. (2007) Characterization and localization of *Plasmodium falciparum* homolog of prokaryotic ClpQ/HslV protease. *Mol. Biochem. Parasitol.* **152,** 139–148
49. Larkin, M. A., Blackshields, G., Brown, N. P., Chenna, R., McGettigan, P. A., McWilliam, H., Valentin, F., Wallace, I. M., Wilm, A., Lopez, R., Thompson, J. D., Gibson, T. J., and Higgins, D. G. (2007) Clustal W and Clustal X version 2.0. *Bioinformatics* **23,** 2947–2948
50. Gouet, P., Courcelle, E., Stuart, D. I., and Métoz, F. (1999) ESPript. Analysis of multiple sequence alignments in PostScript. *Bioinformatics* **15,** 305–308
51. Vaguine, A. A., Richelle, J., and Wodak, S. J. (1999) SFCHECK. A unified set of procedures for evaluating the quality of macromolecular structure-factor data and their agreement with the atomic model. *Acta Crystallogr. D Biol. Crystallogr.* **55,** 191–205
52. Marti, M., Good, R. T., Rug, M., Knuepfer, E., and Cowman, A. F. (2004) Targeting malaria virulence and remodeling proteins to the host erythrocyte. *Science* **306,** 1930–1933
53. McCoy, A. J., Grosse-Kunstleve, R. W., Adams, P. D., Winn, M. D., Storoni, L. C., and Read, R. J. (2007) Phaser crystallographic software. *J. Appl. Crystallogr.* **40,** 658–674